Loss Modeling of Large Hydrogenerators for Cost Estimation of Reactive Power Services and Identification of Optimal Operation

Yannick Cyiza Karekezi, *Student Member, IEEE,* Emil Ghieh Melfald, Thomas Øyvang, *Member, IEEE,* and Jonas Kristiansen Nøland, *Senior Member, IEEE*

***Abstract*— As a result of the worldwide energy transition, reactive power generation has started to become a more scarce resource in the power grid. Until recently, reactive power has been an auxiliary grid service that classical power generation facilities have provided without necessarily allocating any cost for this valuable service. In this paper, a new approach for predicting the additional costs of reactive power services delivered by large hydrogenerators is proposed. We derive the optimal reactive power (ORP) with minimal losses as a function of the active power level within the generator's capability diagram. This pathway can then be used to calculate additional losses from operational regimes deviating from the ORP. To back up the analysis, a dedicated example study was handpicked consisting of four real-world generators scaled in terms of power rating, i.e., $15\,\mathrm{MVA}$, $47\,\mathrm{MVA}$, $103\,\mathrm{MVA}$, and $160\,\mathrm{MVA}$. The objective was to identify how the ORP scale from smaller to larger MVA-sized generators. Moreover, a sensitivity analysis of the machine characteristics is conducted. We find the ratio between the rotor and stator losses as the determining factor. Finally, we show how our framework could justify profit for reactive power services, which are projected to increase in the future.**

***Index Terms*—Synchronous machines, hydrogenerators, cost modeling, loss modeling, reactive power.**

NOMENCLATURE

Δt_i, T	Discrete time interval and overall time, [h] or [s]
η, η_n, η_{max}, η_a	Actual, nominal, maximum, and accumulated average efficiency, [pu] or [%]
$\mathcal{E}_g$, $\mathcal{E}_p$, U_a	No-load emf and armature voltage, [pu] or [V]
A_i, N_z	Weighting factor and number of zones, [pu] or [%]
b_v, k, C_m, m	Linear slope constant and slope, saturation, and exponential constant for saturation
E, E_l, ΔE_l	Produced, lost, and additionally lost energy, [pu] or [GWh]
I_a, I_f, I_{fu}	Armature, field, and unsaturated field current, [pu] or [A]
n, f	Machine speed and frequency, [rpm] and [Hz]
P, $\overline{P}_l$, ΔP_l, $\Delta\overline{P}_l$	Active power, mean loss, additional loss, and mean additional loss, [pu] or [kW]
$P_{l,c}$, P_{be}, P_{wf}, P_c	Total constant, bearing, windage and friction, and core losses, [pu] or [kW]
$P_{l,r}$, P_f, P_{ex}, P_{br}	Total rotor, field winding, exciter, and brush losses, [pu] or [kW]
P_l, $P_{l,s}$, P_a, P_s	Total, stator, armature, and stray load losses, [pu] or [kW]
Q, Q_{opt}, Q_{grid}	Actual and optimal reactive power, and grid-side reactive power [pu] or [Mvar]
X_d, X'_d, X_q, X_p	D-axis, D-axis transient, Q-axis, and Potier reactance, [pu] or [Ω]
X_t,X_l	Step-up transformer reactance and generator leakage reactance, [pu] or [Ω]

Manuscript received 11 July 2022; accepted 17 December 2022. This work was supported by the Research Council of Norway (RCN) under Grant no. 326673 (SysOpt project). Paper no. TEC-00717-2022. (*Corresponding author: Yannick Cyiza Karekezi.*)

Y. C. Karekezi and J. K. Nøland are with the Norwegian University of Science and Technology (NTNU), Trondheim, Norway, and also with the University of South-Eastern Norway (USN), Porsgrunn, Norway (e-mail: yannick.c.karekezi@ntnu.no; ykare@usn.no; jonas.k.noland@ntnu.no; jonas.noland@usn.no).

E. G. Melfald and T. Øyvang are with the University of South-Eastern Norway (USN), Porsgrunn, Norway (e-mail: emil.g.melfald@usn.no; thomas.oyvang@usn.no).

I. INTRODUCTION

THE worldwide energy transition will fundamentally transform the future electricity grid to integrate ever-increasing shares of renewable energy sources (RES). At shorter time scales, the intermittency of RES will mainly be balanced by hybridized, fast-response energy storage solutions [1]–[3]. This is because the ramping capability of hydropower is usually limited to 10-30 % per minute to reduce wear and tear and avoid too high thermal stresses [4]. Nevertheless, hydropower can provide firm dispatchable power allocated over longer time scales and secure the baseload of the grid. In this way, the variability of RES can play well together with the flexibility of reservoir-based hydropower, where hydropower production is held back at high rates of RES production while stepping in to fill the gaps in other periods of energy drought and get increased revenue. As a result, hydropower is projected to be pushed closer to its capability boundaries and beyond in the near future. It might even contribute to more firm backup power shared between multiple countries [5].

Over the last decade, the load cycling intervals of large power plants have changed fundamentally from rated conditions to a diverse set of operating points. This effect is highlighted in [6]–[8], where significant changes resulting

from the German 'Energiewende' can already be noticed. As a result of the worldwide energy transition, hydropower would need to adapt to completely new operational regimes to enable rapid growth of variable RES [6], [9], where both the active power capability but also the reactive power capacity can be significantly extended [10], [11]. These more diverse operating regimes bring new economic costs into consideration, as the overall efficiency now becomes a significant differentiator [8]. Moreover, to deliver more reactive power, rotor cooling has been found to be a major limiting factor [12], which is known as the overheating problem in the thermal management [13], [14]. Accurate information about the stator's thermal footprint is also essential [15], and combined with the cooling arrangement, can establish a thermal network for the whole machine to predict the overall capability [16]. These issues become even more critical if one tries to allocate short-term reactive power, as envisaged by an extended capability diagram [11].

A price must be paid in terms of reduced efficiency resulting from the dispatch of active and reactive power. To quantify the impact of variable operation, an accumulated average efficiency (AAE) model was recently proposed to improve the accuracy in the determination of the power losses [17]. It was proposed as an alternative to the mainstreamed weighted average efficiency (WAE) model [18]–[20]. Nevertheless, the main contribution of this paper is not related to the AAE but rather to how the active losses can be minimized and quantifying the cost of not operating the hydrogenerator optimally. The paper proposes a timely method for the identification of the maximum-efficiency operation of hydrogenerators as a basis for cost estimation of its operating regime based on the reactive power services it provides. The loss modeling presented derives an optimal reactive power profile as a function of active power generation, which can be used to inform the operational characteristic needed to maximize the AAE as the active power generation varies. The identification of the optimal reactive power (Q_{opt}) pathway in the capability diagram can therefore quantify the impact of the reduced machine efficiency based on the variation of reactive power services provided to the grid. Finally, the most profitable operation of large synchronous generators is deduced, which is the basis of the proposed technique to estimate the cost of an operational regime, including reactive power services.

A sensitivity study is also presented to see how the model parameters and inputs affect the machine efficiency and optimal operational path. First, the impact of the synchronous reactances, the Potier reactance, and the armature voltage are analyzed. Then, direct adjustments in the rated stator and rotor power losses are studied to investigate their impacts on the overall performance. The aim is to explore the link between the machine characteristics and the variable machine losses, optimal reactive power, and optimal efficiency. The sensitivity study offers first-order insight into how the different parameters affect the performance quantities under study. Moreover, our paper goes further beyond studying just one particular generator, and looks at the scalability of our findings by investigating a handpicked collection of machines at different ratings. We identify the underlying causes of the optimal reactive power at different scales, which could also provide valuable input to the design strategy from scratch if one wants in this way to influence the optimal generator operation.

The paper is organized as follows. First, Section II presents the presuppositions for the calculations. Then, Section III presents the concept of optimal reactive loading for loss minimization, while section IV presents a sensitivity analysis of the $103\,\mathrm{MVA}$ generator. An example study of four industry generators is provided in Section V. Finally, Section VI presents the clustering of real-world operational data to showcase to what extent calculation simplifications can be made before Sections VII and VIII ends with discussions and conclusions.

II. Key Presuppositions and Assumptions

This section briefly presents the key presuppositions made in the calculations of this paper. They are as follows.

1) All of the operating points inside the capability diagram are assumed to be steady-state. There are no transients or sub-transients captured in the loading conditions.
2) The generator is connected to a large interconnected grid, implying that the voltage is stiff and equal to $1\,\mathrm{pu}$ for all loading points. The generator terminal point of connection is chosen as the reference point. It is, therefore, given the value of $1\,\mathrm{pu}$ and zero degrees as a reference. As a result, the armature current is directly proportional to the apparent power.
3) The synchronous reactance used in this manuscript is the reactance between the induced generator voltage and the generator terminal (i.e., step-up transformer reactance is neglected). Thus, the synchronous reactance in the d-axis is the summation of the direct-axis main reactance and the leakage reactance.
4) The downstream profile of the generator terminals was the main focus of all analyses. Consequently, the production profiles of artificially made uniform and synchronous condenser-dominated load distribution do not consider the upstream grid code requirements, where the step-up transformer could limit the reactive power production [8]. However, our modeling could add the reactance of the simple line equivalent of the step-up transformer to the generator's leakage reactance without changing the model. In this way, we have similarly estimated the grid-side reactive power as presented in [8].
5) The operational regimes presented in this paper assume that there is no large-scale energy storage units other than fast-response storage for balancing RES intermittency at shorter time scales. The hydrogenerator is assumed to have all the dispatchable power reserves needed to dispatch RES at longer time scales. Thus, it highly varies in both active and reactive power levels.

III. Optimal Loading for Loss Minimization

In this section, the concept optimal reactive power (Q_{opt}) for loss minimization will be developed. A loss minima implies maximization of profit for a given active power production

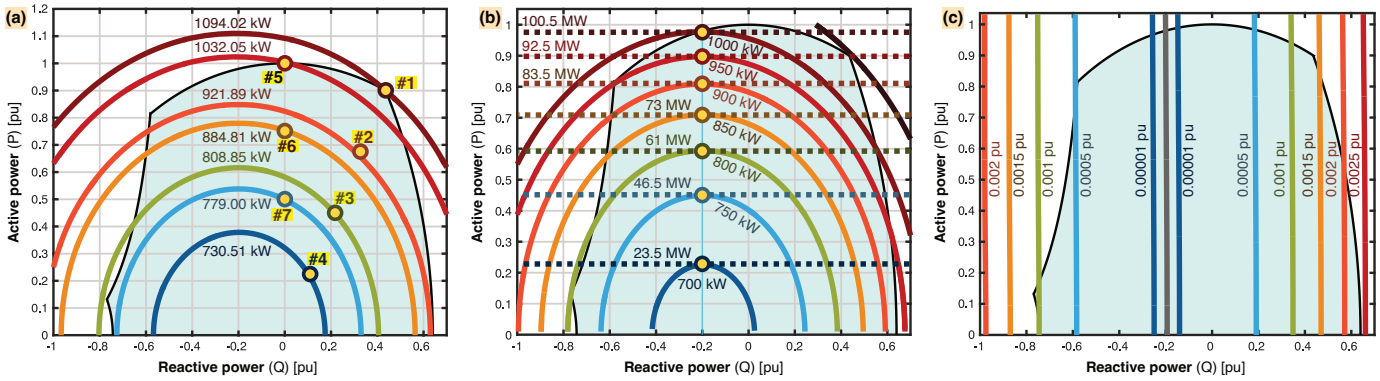

Fig. 1. Case study for a 103 MVA hydropower generator [17]. **(a)**: Measured losses (P_l) for 7 different load points versus predicted loss contours using eq. (7). **(b)**: Combined plotting of power production lines and power loss curves extracted from the loss model. **(c)**: Contour plot of additional losses (ΔP_l) solving eqs. (1) and (2). The losses for each active power level (P) were calculated for the full reactive power (Q) range. Then, the minimum losses were subtracted from the total losses for each active power level. Additional losses occur when deviating from the optimal P-Q load path (indicated in grey).

(P). The total losses (P_l) in the generator is a function of both P and Q. The minima is found by differentiation, yielding

$$\frac{d}{dQ}\left[P_l(Q,P)\right] = 0, \tag{1}$$

where the solution, $Q_{opt}(P)$, is the solution to reactive power enabling the minimum losses as functions of P. Based on this convention, additional losses (ΔP) for a given P can be established based on the distance between Q and Q_{opt}, formulated as $|\Delta Q| = |Q - Q_{opt}|$. We will later observe that ΔP_l is approximately proportional to a second-order polynomial function of $|\Delta Q|$, as indicated in eq. (2).

$$\Delta P_l = P_l(Q,P) - P_l(Q_{opt},P) \approx f(|\Delta Q|) \tag{2}$$

The accumulation of ΔP can be used to quantify the total cost of not operating along the optimal reactive power path.

$$\begin{aligned}\Delta E_l &= \sum_i^n \Delta P_{l,i}\Delta t_i = T\sum_i^n \Delta P_{l,i}A_i = T\overline{\Delta P_l} \\ &= \Delta P_{l,1}\Delta t_1 + \Delta P_{l,2}\Delta t_2 + \ldots + \Delta P_{l,n}\Delta t_n \\ &= T\underbrace{\left(\Delta P_{l,1}A_1 + \Delta P_{l,2}A_2 + \ldots + \Delta P_{l,n}A_n\right)}_{\Delta\overline{P_l}}\end{aligned} \tag{3}$$

Eq. (3) accumulates the additionally wasted energy either using the exact calculation with time intervals or the method using weights representing the probability of occurrence.

To enhance the insights into the loss modeling, this paper separates the losses into rotor, stator, and constant losses as formulated in eqs. (4)-(8) with case values in Table I.

$$P_{l,s} = P_a + P_s = (P_a^* + P_s^*)\left(\frac{I_a}{I_a^*}\right)^2 \tag{4}$$

$$P_{l,r} = P_f + P_{br} + P_{ex} = P_{ex}^*\left(\frac{I_f}{I_f^*}\right) + (P_f^* + P_{br}^*)\left(\frac{I_f}{I_f^*}\right)^2 \tag{5}$$

$$P_{l,c} = P_c + P_{be} + P_{wf} = P_c^*\left(\frac{U_a}{U_a^*}\right)^2 + P_{be}^* + P_{wf}^* \tag{6}$$

$$P_l = P_{l,s} + P_{l,r} + P_{l,c} \tag{7}$$

$$\eta = \frac{P}{P + P_{l,s} + P_{l,r} + P_{l,c}} \tag{8}$$

TABLE I
RECORDED NOMINAL LOSS COMPONENTS USED IN THE LOSS SEPARATION MODEL OF THE 103 MVA, 500 rpm, 11 kV, 50 Hz HYDROGENERATOR

$\mathbf{P_a^* + P_s^*}$	$\mathbf{P_{ex}^*}$	$\mathbf{P_f^* + P_{br}^*}$	$\mathbf{P_c^*}$	$\mathbf{P_{be}^* + P_{wf}^*}$
276.62 kW	15.88 kW	175.78 kW	211.92 kW	413.82 kW

TABLE II
STANDARD PARAMETERS OF THE 103 MVA, 500 rpm, 11 kV, 50 Hz HYDROGENERATOR

$\mathbf{R_a}$	$\mathbf{X_d}$	$\mathbf{X_q}$	$\mathbf{X_p}$	$\mathbf{X_t}$
0.002 pu	1.087 pu	0.676 pu	0.144 pu	0.129 pu

The variables in the loss separation model is I_a, I_f, and U_a, where I_a^*, I_f^*, and U_a^* refer to their nominal values. The armature current is calculated in per unit as $I_a = \sqrt{P^2 + Q^2}/U_a$, while the field current is found from $I_f = f(\mathcal{E}_g, \mathcal{E}_p)$ using the armature reaction parameters of the machine (R_a, X_d, X_q, and X_p in Table II) and the open-circuit saturation characteristics (OCC) [17]. The field current is approximated via the similar simplifications of the Potier method presented in [17]. It is based on the machine parameters and the OCC curve only, which is reduced from more detailed models described in appropriate standards [21].

The loss models are strongly simplified with the assumption that the machine has warm components and is operating at a steady state. Nevertheless, the modeling is well-founded in stationary conditions, even though a warm machine will differ from a cold machine. In the case of a fast dynamic load change, thermal equilibrium needs to settle before the modeled behavior is valid. Moreover, the influence of the operating temperatures on machine losses is neglected, which can strongly affect the field winding losses, in particular. The saturation modeling involved in estimating the field current also makes the field winding losses a sensitive loss component.

A. Initial Case Study of the Hydrogenerator's Loss Minima

By utilizing the machine data of the 103 MVA hydrogenerator provided in Tables I and II, some preview results for the

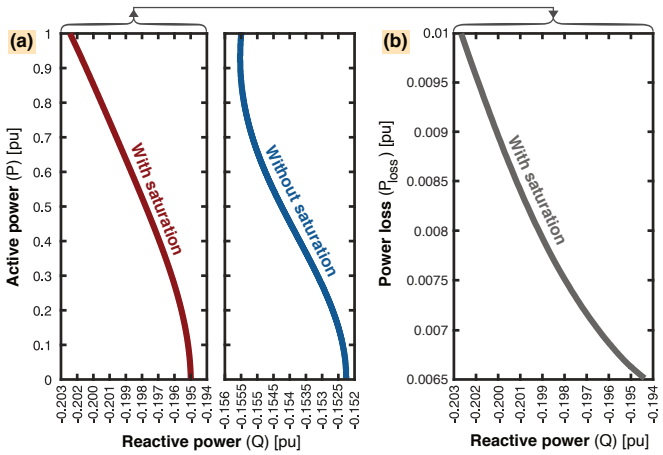

Fig. 2. Solution $Q_{opt}(P)$ of eq. (1) for the loss model of the 103 MVA hydropower generator [17]. **(a)**: Q_{opt} as a function of P with and without saturation (i.e., considering only the air-gap line and neglecting the nonlinear saturation curve). **(b)**: Minimum $P_l(Q_{opt})$ curve for the optimal P-Q in **(a)**.

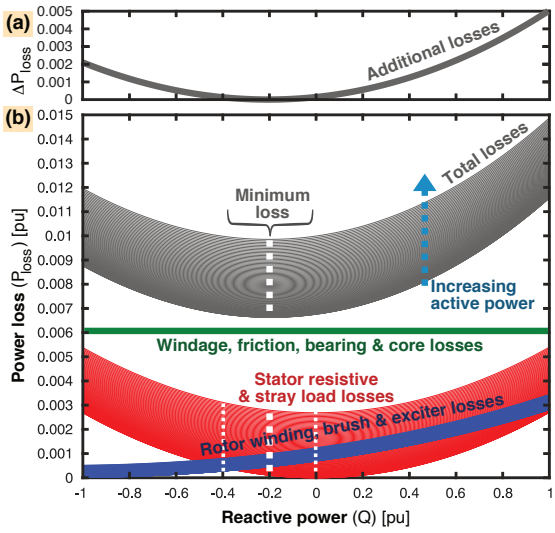

Fig. 3. 1D plots of the contours in Fig. 1-c for 100 P levels between 0 and 1 pu. **(a)**: Difference between the absolute losses and the minimum losses, ΔP_l from eq. (2). **(b)**: Absolute losses, $P_l(Q)$, for different P-levels.

loss minimization and optimal reactive power are provided in Fig. 1. Its power loss contours are validated by seven stationary measurements in Fig. 1-(a). Furthermore, by combining the active power production lines in the capability diagram with the loss curves, an optimal operation path can be proposed, as illustrated in Fig. 1-(b). The active power lines giving the lowest active power losses are those that intersect with the peak of the loss contours, which is about -0.2 pu in reactive power for this particular case. Finally, by subtracting the minimal losses along the optimal P-Q profile, the additional losses are derived in Fig. 1-(c).

Fig. 2-(a) further investigates the $Q_{opt}(P)$ solution of eq. (1), with and without saturation, where the minimum losses are given in Fig. 2-(b). It is shown that one needs to increase the consumption of Q slightly as one increases P. Moreover, Fig. 3 reveals that it is the optimum interaction between the rotor and stator losses that determines Q_{opt}. When extracting out the additional losses from eq. (2), the curves are more or less independent of the active power, as shown in Fig. 3-(a). Moreover, 3-(b) highlights that when plotting the total losses for the full range of active power levels, the shape of the loss profiles is identical with respect to reactive power but has different loss offsets. As a result, the minimum losses for the studied generator is around -0.2 pu reactive power, regardless of the active power level.

B. Basic Cost Modeling of Reactive Power Services

A handpicked average retail electricity price for the US in 2020 is 10.66 ¢/kWh [22], which is taken as the basis for income and cost calculations herein. The income for a given P is multiplied by the price and time (Δt), and the same for the cost associated with the P_l. The gross profit is proportional to the production income minus the loss costs. As a result, the optimal profit strategy is operating at the optimal operation that minimizes P_l. The additional operational costs for a particular load point can be predicted by multiplying $\overline{\Delta P_l}$ from eq. (2) with the electricity price (0.1066 $/kWh) and the number of

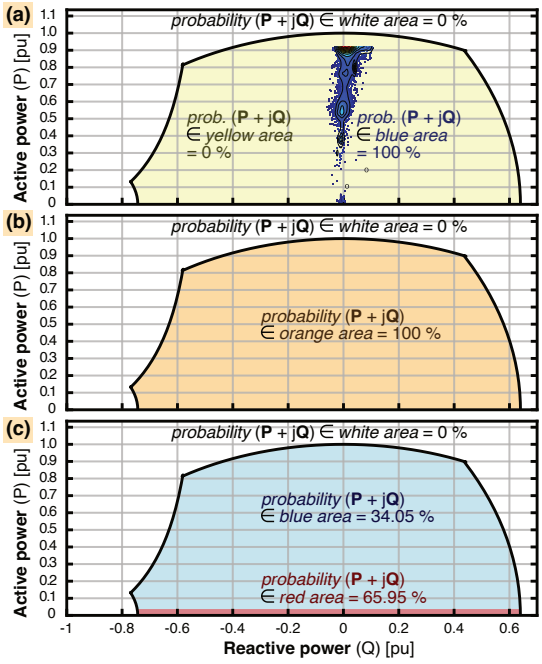

Fig. 4. Three different load distributions investigated in terms of cost of operation for a 103 MVA hydrogenerator. **(a):** Concentrated distribution representing yearly historical operational data for the generator. **(b):** Uniform load distribution where all load points are uniformly distributed inside the capability diagram. **(c):** Synchronous condenser-dominated distribution. The load points in the blue area are uniformly distributed (equal probability of occurrence for all load points), with a 65.95 % probability that a load point operates as a synchronous condenser (red area).

hours (h) of operation. Table III highlights that $Q \approx$ -0.2 pu is the most profitable operating point at rated P.

To expand the preliminary cost modeling in Table III, the impact of three different operational regimes has been assessed in terms of cost. A concentrated distribution of measured data (mostly operating at unity power factor) for a whole year of the 103 MVA is compared against two distributions, all

TABLE III
INCOME, COST AND PROFIT FOR SIX REACTIVE POWER LOADS AT NOMINAL ACTIVE POWER FOR THE 103 MVA HYDROGENERATOR

Load point	**#1**	**#2**	**#3**	**#4**	**#5**	**#6**
Reactive power (Q) (terminals)[a]	−0.400 pu	−0.200 pu	0.000 pu	0.200 pu	0.400 pu	0.600 pu
Reactive power (Q_{grid}) (grid connection)[b]	−0.525 pu	−0.310 pu	−0.104 pu	0.090 pu	0.275 pu	0.449 pu
Additional loss (normalized value) (ΔP_l)	$1.31 * 10^{-4}$pu	0.00 pu	$1.36 * 10^{-4}$pu	$5.44 * 10^{-4}$pu	0.0012 pu	0.0022 pu
Additional loss (absolute value) (ΔP_l)	13.49 kW	0.00 kW	14.01 kW	56.03 kW	123.60 kW	226.60 kW
Additional lost energy per year (ΔE_l)	0.118 GWh	0.000 GWh	0.123 GWh	0.491 GWh	1.083 GWh	1.985 GWh
Production income	9881.80 $/h	9881.80 $/h	9881.80 $/h	9881.80 $/h	9881.80 $/h	9881.80 $/h
Loss cost	102.90 $/h	101.50 $/h	102.95 $/h	107.4 $/h	114.95 $/h	125.56 $/h
Net profit	9778.90 $/h	9780.40 $/h	9778.90 $/h	9774.4 $/h	9766.9 $/h	9756.3 $/h

[a] Constant inputs for every load point considered: U_a = 1 pu and P = 0.9 pu. [b] Using eqs. (5) and (6) in [8].

TABLE IV
ADDITIONAL LOSS, INCOME, COST AND PROFIT OF THE 103 MVA HYDROGENERATOR FOR THE THREE DIFFERENT LOAD DISTRIBUTIONS IN FIG. 4

Distribution	**E**	**E_l**	**ΔE_l**	**$\overline{P}_l$**	**$\Delta\overline{P}_l$**	**Production income**	**Loss cost**	**Net profit**
Concentrated dist.	652.175 GWh	7.715 GWh	0.155 GWh	0.0087 pu	$1.747 * 10^{-4}$ pu	69.522 M$	0.822 M$	68.7 M$
Uniform load dist.	401.926 GWh	7.239 GWh	0.484 GWh	0.0080 pu	$5.081 * 10^{-4}$ pu	42.850 M$	0.770 M$	42.080 M$
Synchronous cond. mode	148.290 GWh	6.780 GWh	0.516 GWh	0.0075 pu	$5.716 * 10^{-4}$ pu	15.812 M$	0.7214 M$	15.091 M$

The exact AAE for the measured concentrated distribution is 98.83 % with 8610 data points (see Fig. 4), the calculated AAE for uniformly distributed load is 98.23 with 11489 load points with equal weight (over the whole capability diagram), and the AAE for synchronous condenser mode is 95.63 % with 12808 load points (uniformly distributed with synchronous condenser operation weighted to be 65.95 % of the time).

depicted in Fig. 4. Table IV reveals that the most profitable operational regime is a concentrated load distribution due to a high income and relatively low operational cost because it mostly operates close to Q_{opt}. In contrast, the synchronous condenser-dominated mode has the lowest profit due to long periods of low P, but it also has more than three times more additional losses and costs due to its reactive power services.

IV. PARAMETER SENSITIVITY TO THE LOSS MODELING

To gain a deeper understanding of the underlying modeling mechanisms determining the optimal reactive power, a parametric sensitivity study is done of the 103 MVA hydrogenerator. The analysis is conducted in normalized quantities, which means that the same principles apply to other generators, yielding a level of generalisability. The parameters under study, namely X_d, X_q, X_p, and U_a, are altered to affect the machine efficiency and consequently change the optimal reactive power (Q_{opt}), using the loss model presented in eqs. (4)-(7). In Table V, three different values for each parameter under study are investigated, highlighting changes in losses, efficiency, and optimal reactive power. When one of the parameters changes, the other ones are kept constant at the original value according to Table II. Furthermore, another simplification is made assuming that the standard parameters X_d, X_q, and X_p are not affecting the no-load curve of the machine in the sensitivity study, where $I_f \approx (\mathcal{E}_g - \mathcal{E}_p)/b_v + k(\mathcal{E}_p + C_m \mathcal{E}_p^m)$ [17]. Nevertheless, the parameters at the design stage are very much correlated with each other. The sensitivity analysis results are also plotted in Fig. 5.

There is a slight negative trend between the reactance values (X_d, X_q, X_p) and the machine efficiency. Higher synchronous reactances (X_d and X_q) increase both the induced voltage ($\mathcal{E}_g$) and the Potier voltage magnitude ($\mathcal{E}_p$) and angle. Thus, the field current is increased and indirectly affected. This again leads to higher rotor losses according to eq. (5). However, the reactance values do not influence the stator losses nor the other constant losses in this simplified modeling approach. The physical limitation is that, in reality, the stray load losses would be affected due to the armature reaction's magnetomotive force depending on the air gap, which is influenced by X_d and vice versa.

A change in the armature voltage has the overall largest impact on the efficiency and Q_{opt}. E.g., increasing the armature voltage causes a decrease in the armature current, consequently reducing stator losses. However, both rotor and constant losses are, in general, increasing from higher values of U_a. As seen from Fig. 5, the efficiency is highest around nominal condition (U_a = 1.0).

The AAE for the three operational regimes described in Fig. 4 stays mostly constant in relation to each other. Machine reactances do not affect the AAE in any significant way. The armature voltage has the largest impact on the AAE, while the load distribution is a more substantial factor.

A. Sensitivity to Changes in Rotor and Stator Losses

A second part of the sensitivity study is presented in Table VI and Fig. 6. The rotor and stator losses at the nominal point (described in Table I) are incrementally increased from their default value using an adjustment factor. This is done to see how the optimal reactive power and efficiency are affected when either the rotor or stator losses become more dominant. The rated losses in the stator and the rotor are scaled directly in the calculation and adjusted from their original values. This can be seen quantitatively in Table VI and in Fig. 6. By increasing the stator losses, the optimal reactive power moves asymptotically toward zero (i.e., the unity power factor is optimal). However, when stator losses approach zero, the optimal reactive power will exceed -1 pu and will then

TABLE V
SENSITIVITY ANALYSIS OF THE STANDARD PARAMETERS IN TABLE II FOR THE NOMINAL OPERATING POINT OF S = 1.0, $\cos\varphi$ = 0.9 (INDUCTIVE)

		$\mathbf{X_d}$			$\mathbf{X_q}$			$\mathbf{X_p}$			$\mathbf{U_a}$		
Symbol	**Default**	**0.8 pu**	**1.1 pu**	**1.4 pu**	**0.4 pu**	**0.7 pu**	**1 pu**	**0.1 pu**	**0.3 pu**	**0.8 pu**	**0.95 pu**	**1 pu**	**1.05 pu**
$P_{l,s}$ [pu]	0.0027	0.0027	0.0027	0.0027	0.0027	0.0027	0.0027	0.0027	0.0027	0.0027	0.0030	0.0027	0.0024
$P_{l,r}$ [pu]	0.0019	0.0018	0.0019	0.0019	0.0015	0.0019	0.0024	0.0018	0.0023	0.0035	0.0017	0.0019	0.0020
$P_{l,c}$ [pu]	0.0061	0.0061	0.0061	0.0061	0.0061	0.0061	0.0061	0.0061	0.0061	0.0061	0.0059	0.0061	0.0063
P_l [pu]	0.0107	0.0106	0.0107	0.0107	0.0103	0.0107	0.0112	0.0106	0.0111	0.0123	0.0106	0.0107	0.0107
η_n [%]	98.834	98.843	98.833	98.830	98.870	98.827	98.780	98.840	98.791	98.659	98.836	98.834	98.820
Q_{opt} [pu]	-0.2015	-0.2146	-0.2004	-0.1933	-0.167	-0.2068	-0.2444	-0.1945	-0.2264	-0.2602	-0.1728	-0.2015	-0.2362
η_{opt} [%]	98.984	98.998	98.983	98.978	98.996	98.982	98.968	98.983	98.984	98.981	98.985	98.984	98.975

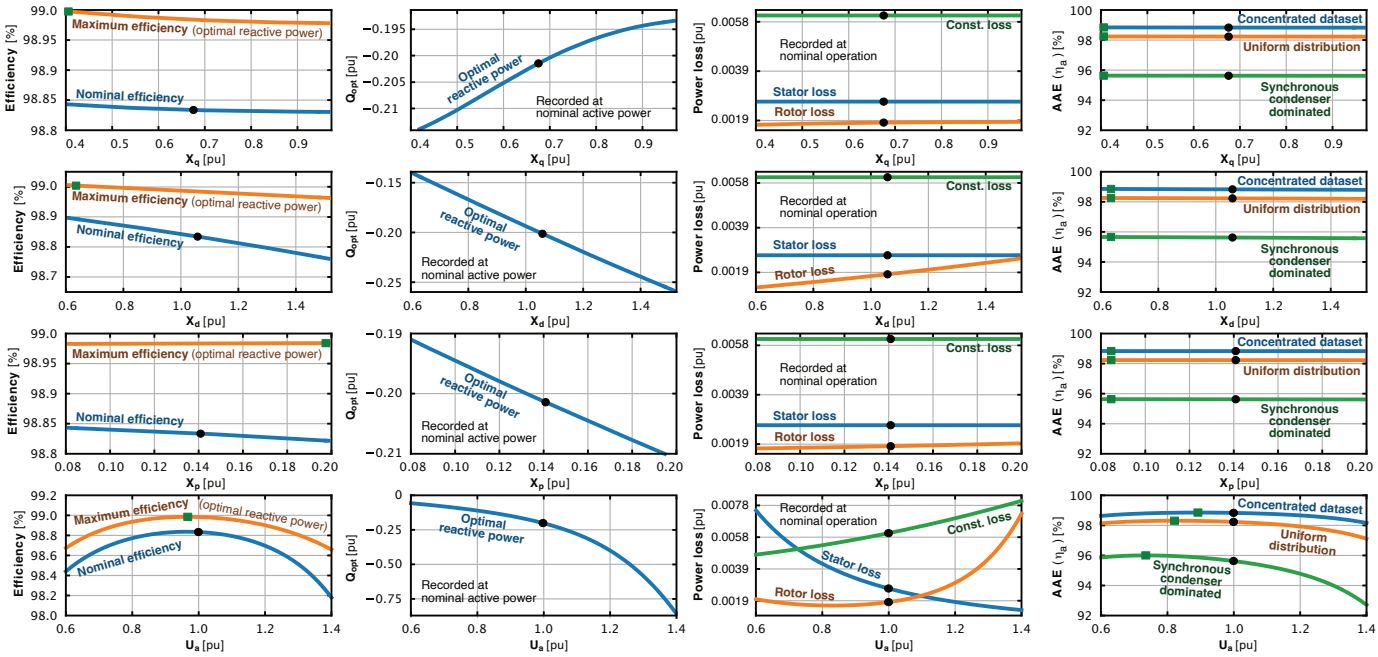

Fig. 5. Efficiency, optimal reactive power, and losses as the standard parameters X_d, X_q, X_p, and U_a are changed for the 103 MVA hydrogenerator.

TABLE VI
THE IMPACT OF ALTERING THE RATED STATOR AND ROTOR LOSSES ON THE OPTIMAL REACTIVE POWER AND THE AAE OF DISTRIBUTIONS IN FIG. 4

Adjustment factor	**Symbol**	**Description**	**Adjustment factor 0.1**	**0.5**	**1.0 (Default)**	**1.5**	**2.0**
$P_{l,s}/P^*_{l,s}$	Q_{opt}	Reactive power with loss minima	−0.7558 pu	−0.3378 pu	−0.2015 pu	−0.1438 pu	−0.1119 pu
	η_{max}	Efficiency with optimal Q	99.237 %	99.112 %	98.984 %	98.861 %	98.741 %
	η_a	AAE with concentrated dataset	99.021 %	98.937 %	98.832 %	98.727 %	98.622 %
		AAE with uniform load distribution	98.441 %	98.347 %	98.231 %	98.114 %	97.998 %
		AAE with synchronous condenser distr.	95.960 %	95.811 %	95.626 %	95.442 %	95.259 %
$P_{l,r}/P^*_{l,r}$	Q_{opt}	Reactive power with loss minima	−0.0246 pu	−0.1119 pu	−0.2015 pu	−0.2754 pu	−0.3378 pu
	η_{max}	Efficiency with optimal Q	99.08 %	99.034 %	98.984 %	98.938 %	98.896 %
	η_a	AAE with concentrated dataset	98.956 %	98.900 %	98.832 %	98.763 %	98.694 %
		AAE with uniform load distribution	98.401 %	98.325 %	98.231 %	98.136 %	98.042 %
		AAE with synchronous condenser distr.	96.018 %	95.844 %	95.626 %	95.410 %	95.195 %

be constrained by the outer limits of the capability diagram. In contrast, zero rotor loss implies that the optimal reactive power of the generator is 0 pu. These findings provide valuable insight into what determines the optimal reactive power in the trade-off between the stator and rotor losses. To expand on these preliminary insights, an example study of several generators of different sizes and characteristics will be the focus of the next section.

V. EXAMPLE STUDY OF FOUR INDUSTRY GENERATORS

This section presents an example study consisting of four power industry generators, i.e., G1, G2, G3, and G4, where generator G2 represents the already investigated preliminary study case. To generalise the findings, a comparative study of the optimal reactive loading of generators is provided.

A. Measured Performance Data

The key rated quantities of G1-G4 can be seen in Table VII, and the rated losses of each generator are provided in Table

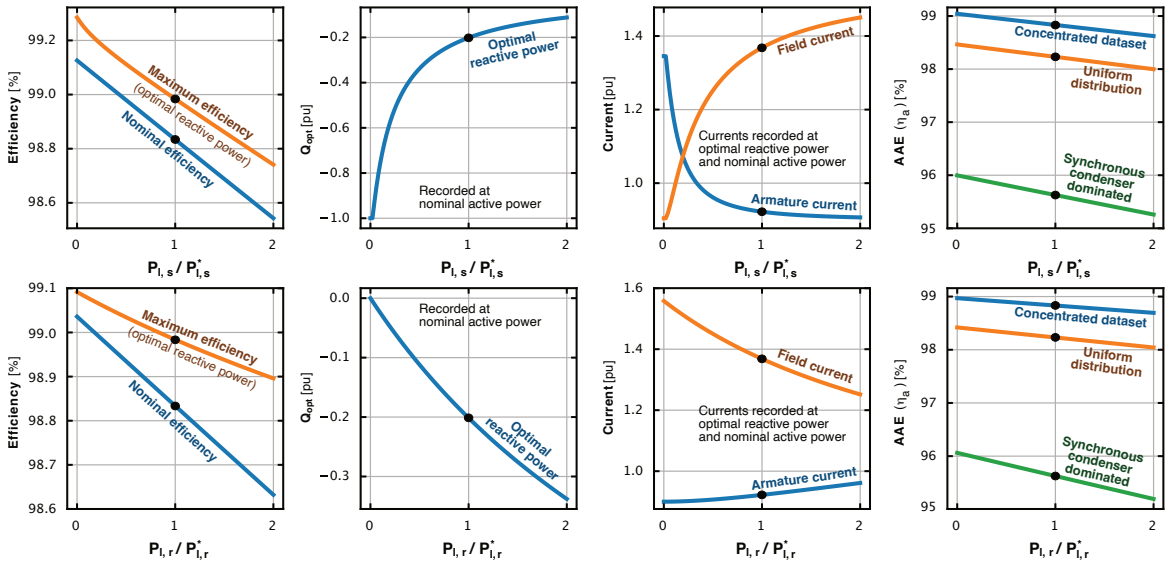

Fig. 6. Mapping of the sensitivity characteristics of the 103 MVA hydrogenerator (associated plots to Table VI); Maximum efficiency (η_{max}), optimal reactive power (Q_{opt}), armature current (I_a), field current (I_f), and AAE (η_a) as a function of scaling the stator and rotor nominal losses by adjustment factors ($P_{l,s}/P^*_{l,s}$ and $P_{l,r}/P^*_{l,r}$). These factors are equal to unity in the default case. The nominal point for the loss scaling was P = 0.9 pu and Q = 0.436 pu.

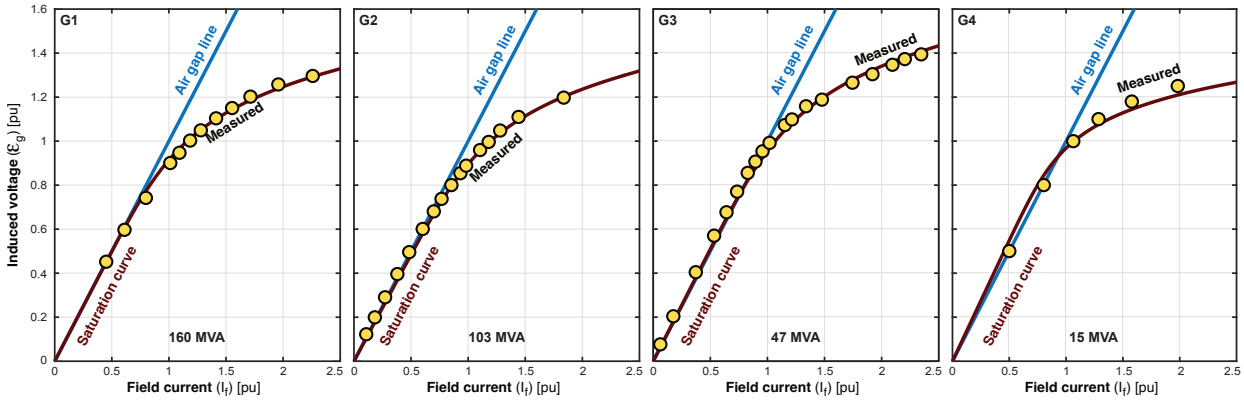

Fig. 7. Modeled, $I_f = k(\mathcal{E}_g + C_m\mathcal{E}_g^m)$ [17], versus the measured OCC of G1-G4 in the example study. The base value for the plots are the airgapline rated field current (I_{fu}) and the rated terminal voltage (U_a) (see Table VII). The modeled OCC curves are based on coefficients provided in Table IX.

TABLE VII
KEY QUANTITIES OF THE GENERATORS IN THE EXAMPLE STUDY

Symbol	G1	G2	G3	G4
S_b	160 MVA	103 MVA	47 MVA	15 MVA
cos (φ)	0.95	0.90	0.90	0.90
η_n	98.41 %	98.834 %	98.20 %	98.09 %
U_a	15 kV	11 kV	11 kV	10.5 kV
I_a	5406 A	5406.1 A	2467 A	824.8 A
I_f	1047.0 A	1065.0 A	1156.0 A	553.9 A
I_{f0}	594.0 A	525.15 A	592.7 A	262.7 A
f	50 Hz	50 Hz	50 Hz	50 Hz
n	150.0 rpm	500 rpm	166.67 rpm	500 rpm
X_d	0.8 pu	1.059 pu	0.867 pu	1.153 pu
X_q	0.6 pu	0.676 pu	0.621 pu	0.726 pu
X_p	0.18 pu	0.141 pu	0.258 pu	0.1939 pu
R_a	0.002 322 pu	0.001 82 pu	0.0032 pu	0.005 47 pu

TABLE VIII
RECORDED NOMINAL LOSSES FOR OF GENERATORS G1-G4

Generator	G1	G2	G3	G4
P_f	477.81 kW	173.65 kW	158.2 kW	61.4 kW
P_{ex}	33.96 kW	15.88 kW	17.6 kW	5.0 kW
P_{br}	5.3 kW	2.13 kW	0.0 kW	1.1 kW
P_a	327.05 kW	187.46 kW	184.9 kW	82.1 kW
P_s	237.07 kW	89.16 kW	101.8 kW	26.0 kW
P_c	539.87 kW	211.92 kW	156.6 kW	53.3 kW
P_{be}	156.17 kW	240.90 kW	52.0 kW	20.0 kW
P_{wf}	710.47 kW	172.92 kW	156.7 kW	14.0 kW
$P_{l,tot}$	2488.33 kW	1094.02 kW	776.8 kW	262.9 kW
η_n	98.41 %	98.834 %	98.20 %	98.09 %

VIII. When not explicitly known, the Potier reactance, which is useful to estimate the field current in loaded conditions, was estimated using the approximation where $X_p \approx 0.7X_d^{'}$ [23], which applies for generators G2 and G4. The reported measured losses were evaluated according to the guidelines of the IEC 60034-1 [24] and IEC 60034-2-3 [25], respectively.

TABLE IX
FIELD CURRENT MODELING COEFFICIENTS FOR G1-G4

Generator	$\mathbf{b_v}$	$\mathbf{C_m}$	$\mathcal{E}_\mathbf{g}$	$\mathbf{m}$	$\mathbf{k}$
G1	1	0.016	0 - 1.3	7	1.0
G2	1	0.160	0 - 1.8	7	1.0308
G3	1	0.09	0 - 1.6	7	0.98
G4	1	0.175	0 - 1.7	9	0.91

TABLE X
OPTIMAL REACTIVE POWER (Q_{opt}) AT RATED POWER OF GENERATORS G1-G4 TAKEN AS A NUMERICAL SOLUTION OF EQ. (1)

	G1	G2	G3	G4
Generator-side	$-0.220\,\mathrm{pu}$	$-0.201\,\mathrm{pu}$	$-0.182\,\mathrm{pu}$	$-0.181\,\mathrm{pu}$
Grid-side[a]	$-0.331\,\mathrm{pu}$	$-0.311\,\mathrm{pu}$	$-0.291\,\mathrm{pu}$	$-0.290\,\mathrm{pu}$

[a] Using eqs. (5)-(6) in [8]. U_a = 1 pu and X_t = 0.129 pu for G1-G4.

B. Extraction of Open-Circuit Characteristics

The open-circuit characteristics (OCC) of generators G1-G4 are modeled using coefficients presented in Table IX, which are used to be matched against the measured data [17], [26]. The air gap line and the OCC are found using [27] and the OCC data for G1-G4 are given in the standard datasheets of these real-world generators. Already, G2 and G3 are provided in [17] and [28], respectively. The estimated OCC profiles for G1-G4 are compared against the recordings in Fig. 7. It can be noted that there are some deviations between the model fit and the measurements because the unsaturated and saturated part of the OCC is modeled with a unified approximation that covers all regions, i.e., $I_f \approx k(\mathcal{E}_g + C_m \mathcal{E}_g^m)$.

C. Detailed Example Study of Optimal Reactive Loading

The validation of the iso-efficiency maps of G1-G4 is presented in Fig. 8, which are used to verify the calculation by experimentally cross-checking the calculated curves against the measured efficiencies given at specific load points. Moreover, the optimal reactive power operations (Q_{opt}) of the four industry generators are visualized in Fig. 9. They highlight how the exact optimal reactive path differs for the four hydrogenerators with different characteristics. Fig. 9 also presents the separated stator, rotor, and constant losses, in addition to the total losses, which provide further insights into how the total losses are distributed. What is noticeable is that even though the losses vary, the overall loss curve for all the different generators still has a minimum value of very close to -0.2 pu reactive power, as already found in the preliminary study. These values of Q_{opt} are summarized in Table X for nominal active power, where also the corresponding grid-side values have been approximated.

VI. SIMPLIFIED LOSS MODELING OF OPERATIONAL DATA

When the optimal reactive power has been identified for a particular generator, the additional losses and costs from reactive services can be established. The estimation of those can be made easier based on justified simplifications of real-world operational data. The power industry is currently using a method of zone clustering [19], with probability-of-occurrence maps of a specified resolution. However, the error from this simplification has not been explored in terms of loss and cost modeling or through efficiency evaluation. The power producer manually determines the number of clustered zones, with more zones leading to more accurate representations of the operational area. Usually, the real-world data contains a load distribution dataset that tracks the synchronous generator load point every hour (or more often) for a whole year. Ideally, it could contain 8765 distinct operating points for an hourly-based time interval resolution over a whole year. The processing of the data leads to a probability map based on the number of distinct load points inside each zone (i). Each zone's weight or likelihood (A_i) are determined as $A_i = \frac{\Delta t_i}{T}$, where Δt_i is the accumulated time of operation inside zone (i), and T is the total time. The evaluation of the accumulated loss and operational costs of each zone is taken at the center point of each zone.

Table XI assesses the precision of clustering the data in the concentrated dataset that are identical to Fig. 4-(a). The accuracy is shown to be strongly dependent on the number of weighted zones, which approximates the production dataset. Four sample cases of zone resolutions are depicted in Fig. 10. From Fig. 11 and Table XI, we can conclude that the practice of zone clustering is a viable solution. However, suppose the zones do not correctly approximate the clustering of the load points. In that case, it comes at the expense of the efficiency calculation, which would then lead to inaccuracies in the loss modeling, and, consequently, also impact the estimation of the costs of the reactive power service that the generator provides. A more computationally expensive practice is to use all the actual operating points in the loss calculation. In Fig. 11, the AAE (η_a) starts to converge as the number of zones is increased, where it begins to approximate the load density of the concentrated dataset correctly. Even though a lower number of zones overestimates the AAE, it underestimates the mean loss ($\overline{P}_l$) of the data, which also underestimates to cost of the reactive power service the generator provides throughout the year. Still, a realistic estimation of machine losses can be achieved through the clustering of operational data. However, the accuracy of such approximate models is quite dependent upon the number of weighted zones. It is, therefore, important to treat a specific dataset correctly according to its distribution.

TABLE XI
A QUANTITATIVE DEMONSTRATION OF THE RELATIONSHIP BETWEEN THE NUMBER OF ZONES, THE ACTUAL AAE, AND THE MEAN LOSSES, WHERE $\eta_{a,ref}$ = 98.8308 %, $\overline{P}$ = 0.7354 pu AND $\overline{P}_{l,ref}$ = 0.0087 pu

Description	Value			
N_z	10	768	1546	2485
η_a	98.9079 %	98.8956 %	98.8650 %	98.8351 %
$\overline{P}_l$	0.0081 pu	0.0082 pu	0.0084 pu	0.0087 pu
Loss deviation	-6.8966 %	-5.7471 %	-3.4483 %	0.0000 %

VII. DISCUSSION

This paper's proposed approach is able to track the optimal reactive power for a given active power to maximize the efficiency within the capability diagram of the hydrogenerator.

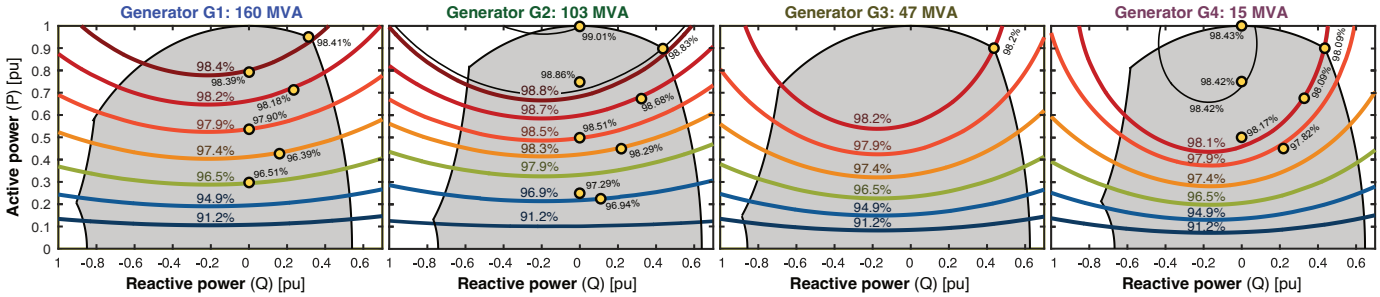

Fig. 8. Iso-efficiency mapping of the four power industry generators validated against measurements.

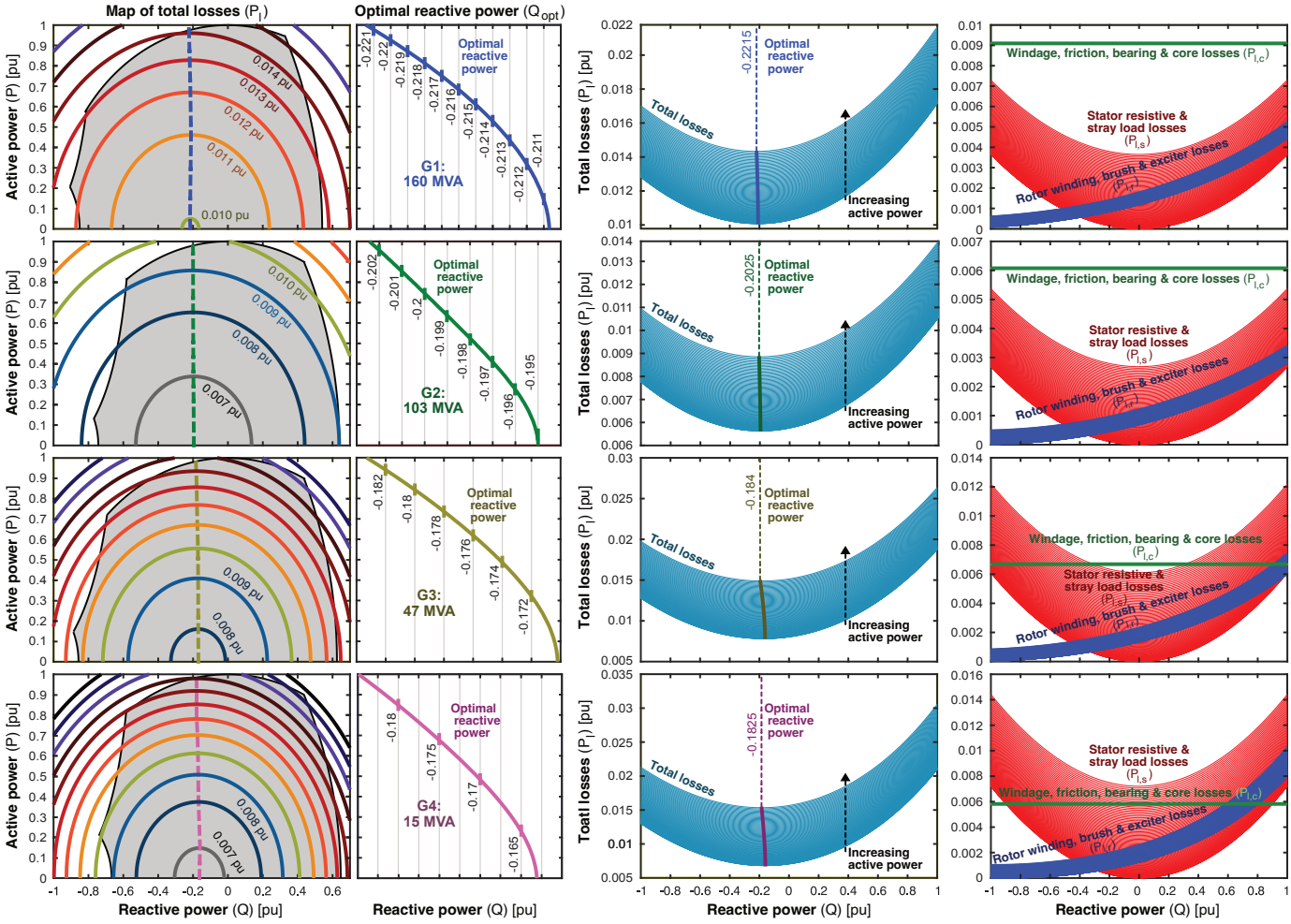

Fig. 9. Mapping of the total losses (P_l), in addition to the varying stator, total rotor, and constant losses separately ($P_{l,s}$, $P_{l,r}$, and $P_{l,c}$). The exact course of the optimal reactive path (Q_{opt}) for all four industry generators, G1-G4, are presented from the top to bottom. E.g., the top row shows the total loss mapping, exact Q_{opt}, separated losses and total losses at different active power levels for generator G1.

However, in the context of the power system, one will not be able to select the optimal reactive power but rather serve the power grid. Nevertheless, the cost of operating non-optimally within the capability diagram can be quantified by identifying the optimal reactive power.

It has also been identified that the coupling between both the rotor and stator performances becomes the primary deciding factor for optimal operation. In particular, the stator and rotor losses directly originate from the stator and rotor designs and their associated parameters. A sensitivity study focused on the uncertainty of how the optimal reactive path is affected when machine parameters and loss distributions are altered. However, it is evident from the design stage that there is a strong correlation between the machine parameters. Nevertheless, the relative altering of individual parameters is valuable in providing insights into parameter sensitivities. Moreover, it gives an in-depth understanding of how isolated changes will influence overall performance.

For general applicability, the optimal reactive paths are investigated at different scales of machine sizes and ratings.

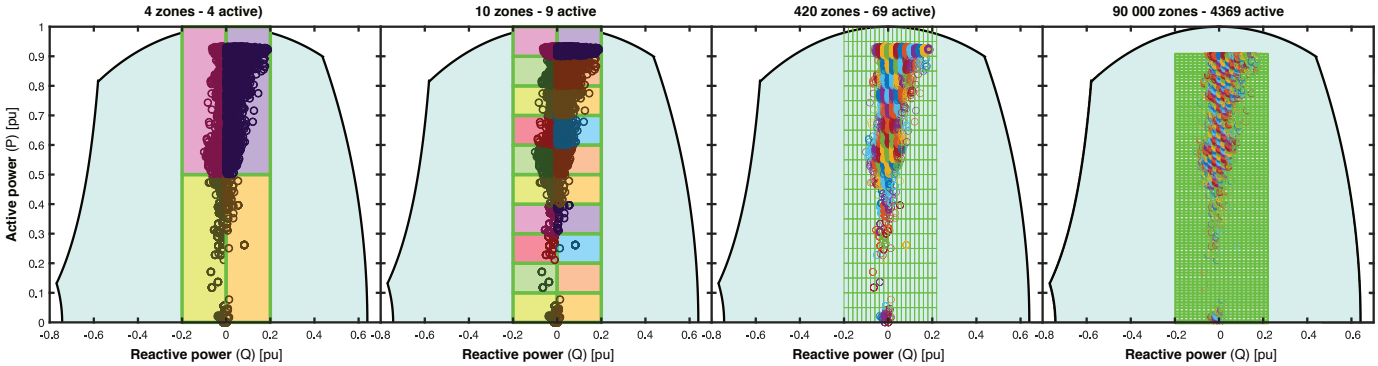

Fig. 10. Illustration of clustering real-world operational data based on zone classification for the Åbjøra power plant (i.e, 103 MVA hydrogenerator), showcased for 4, 9, 420 and 4369 active zones (i.e., zones containing load points), respectively, obtained from the University of South-Eastern Norway.

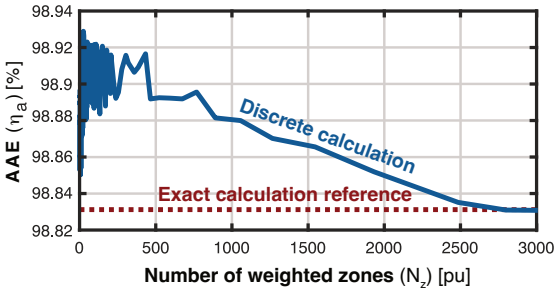

Fig. 11. Impact of the AAE efficiency for a yearly dataset of Åbjøra hydropower plant (i.e, 103 MVA hydro generator) for an increasing number of weighted zones, using the AAE method developed in [17].

The generators under study were generally optimized for overexcited loading conditions (i.e., $\cos(\varphi) \leq 0.9$, inductive). Results show that the optimal reactive path is a consequence of the design, as the exact optimal reactive path differs slightly from case to case. It is evident that when machine size changes, so will the machine parameters, copper and iron weight, and field and armature current loading change accordingly. However, such scaling effects have less impact on the optimal reactive power, which seems to remain more or less unchanged.

Different operational regimes have been investigated to provide enhanced near-term revenue possibilities of reactive power services for power producers. The results presented indicate that deviation from the optimal operation could result in incentives that substantiate an increased revenue for power producers. It can support decision-making for power plant operators and allow them to compare additional losses against revenue for the provision of reactive power. However, it depends strongly on country-specific ancillary service policies. Moreover, the concentrated dataset with high active power production targets a reactive power close to the optimal path and is to be desired to reduce the cost of operation. Compensation for any sub-optimal operation might be an important topic when considering future operational regimes that tend to be less concentrated within the capability diagram. We also show that the cost of reactive power services can be established either by evaluating specific load points or complete operating regimes, where simplifications, such as zone clustering, apply.

VIII. Conclusion

This paper presents a methodology to identify and reveal an operation profile within the capability diagram of hydrogenerators to achieve optimal reactive power dispatch. Our work is based on an example study of four generators of different sizes and ratings, where a comparison is made based on loss modeling and verification against measured data. Finally, we provide evidence for proof-of-concept in terms of cost modeling of reactive power services. The main highlights from our paper are as follows.

1) The model is reasonably accurate for steady-state operation but will differ for a cold machine or in the case of a recent dynamic response. I.e., temperature dependency on losses is neglected.
2) The optimal reactive path referred to the generator terminals is around $-0.2\,\mathrm{pu}$ reactive power for the generators studied in this example study. Nevertheless, the optimal reactive path is always a consequence of the machine design.
3) In general, one can say that the optimal reactive path will always be $\leq 0\,\mathrm{pu}$ in reactive power because the minimum stator losses are at zero reactive power. Moreover, the optimum reactive power will also be $\geq -1\,\mathrm{pu}$ because the minimum rotor losses occur when there is a complete consumption of reactive power at the left border of the capability diagram.

Future work will focus on combining the optimal reactive path of the machine with grid and turbine models in an overall loss minimization framework. Moreover, the modeling framework could further be combined with an advanced control system for optimal operation. Such a control system will be relevant for enhanced system operational security and could help avoid voltage collapses of interconnected power systems.

References

[1] T. Bocklisch, "Hybrid energy storage systems for renewable energy applications," *Energy Procedia*, vol. 73, pp. 103–111, 2015.
[2] T. S. Babu, K. R. Vasudevan, V. K. Ramachandaramurthy, S. B. Sani, S. Chemud, and R. M. Lajim, "A comprehensive review of hybrid energy storage systems: Converter topologies, control strategies and future prospects," *IEEE Access*, vol. 8, pp. 148 702–148 721, 2020.
[3] Y. A. Santos, M. P. M. Nunes, L. A. C. Lemes, and E. C. Bortoni, "Evaluation of hybrid energy storage systems using wavelet and stretched-thread methods," *IEEE Access*, vol. 8, pp. 171 882–171 891, 2020.

[4] M. Joshi, J. D. Palchak, S. Rehman, S. Soonee, S. Saxena, and S. Narasimhan, "Ramping up the ramping capability: India's power system transition," National Renewable Energy Lab.(NREL), Golden, CO (United States); Power ..., Tech. Rep., 2020.
[5] T. Tellefsen, J. van Putten, and O. Gjerde, "Norwegian hydropower: Connecting to continental europe," *IEEE Power Energy Mag.*, vol. 18, no. 5, pp. 27–35, 2020.
[6] J.-H. Braam, "Development, test and validation of new generator product line for current and future operational regimes," in *Proc. Cigre*, 2018.
[7] A. Joswig, K. Walli, and M. Baca, "Synchronous rotating equipment as backbone for renewables," in *Proc. High Volt. Tech. Symp.* VDE, 2018.
[8] J. K. Nøland, M. Leandro, A. Nysveen, and T. Øyvang, "Future operational regimes of bulk power generation in the era of global energy transition: Grid codes, challenges and open issues," in *Proc. IEEE Power Energy Soc. Gen. Meet. (PESGM)*, 2020, pp. 1–5.
[9] W. Yang, P. Norrlund, L. Saarinen, A. Witt, B. Smith, J. Yang, and U. Lundin, "Burden on hydropower units for short-term balancing of renewable power systems," *Nature Com.*, vol. 9, no. 1, pp. 1–12, 2018.
[10] C. Carounagarane, T. R. Chelliah, and D. Khare, "Analysis on thermal behavior of large hydrogenerators operating with continuous overloads," *IEEE Trans. Ind. Appl.*, vol. 56, no. 2, pp. 1293–1305, 2020.
[11] T. Øyvang, J. K. Nøland, R. Sharma, G. J. Hegglid, and B. Lie, "Enhanced power capability of generator units for increased operational security using NMPC," *IEEE Trans. Power Syst.*, vol. 35, no. 2, pp. 1562–1571, 2020.
[12] N. V. Korovkin, D. Verkhovtsev, and S. Gulay, "Rotor air-cooling efficiency of powerful turbogenerator," *IEEE Trans. Energy Convers.*, vol. 36, no. 3, pp. 1983–1990, 2021.
[13] H. Jichao, S. Yutian, Z. Ping, Q. Haiming, D. Jiechen, L. Yufei, Z. Chunli, G. Baojun, and L. Weili, "Influence of complex fluid flow on temperature distribution in the rotor region of large hydrogenerator under the rotor rotation," *IEEE Access*, vol. 10, pp. 3252–3262, 2022.
[14] H. Jichao, L. Yufei, D. Jiechen, S. Yutian, G. Baojun, and L. Weili, "Thermal modeling and experimental validation in the rotor region of hydrogenerator with different rotor structures," *IEEE Access*, vol. 9, pp. 120 001–120 009, 2021.
[15] P. Yang, Y. Liang, X. Bian, and C. Zhou, "3-D thermal network model of stator transposed strands for a hydrogenerator," *IEEE Trans. Ind. Appl.*, vol. 57, no. 1, pp. 218–225, 2021.
[16] H. Wen, Y. Shi, L. Wu, Y. Du, and Y. Fang, "Improving combined flow and thermal network accuracy for radially air-cooled generators by considering the nonlinear resistance characteristics of t-junction flow," *IEEE Trans. Ind. Appl.*, vol. 58, no. 3, pp. 3394–3404, 2022.
[17] Y. C. Karekezi, T. Øyvang, and J. K. Nøland, "The energy transition's impact on the accumulated average efficiency of large hydrogenerators," *IEEE Trans. Energy Convers.*, pp. 1–11, 2022.
[18] E. d. C. Bortoni, R. T. Siniscalchi, S. Vaschetto, M. A. Darmani, and A. Cavagnino, "Efficiency mapping and weighted average efficiency for large hydrogenerators," *IEEE Open J. Ind. Appl.*, vol. 2, pp. 11–20, 2021.
[19] E. Agneholm and et. al., "Report on coordination of grid codes and generator standards: Consequences of diverse grid code requirements on synchronous machine design & standards," *PES-TR69*, Feb 2019.
[20] E. C. Bortoni, M. K. I. Uemori, B. T. Araujo, J. V. Bernardes, J. J. Rocha E., and R. T. Siniscalchi, "Accurate methodology to obtain efficiency mapping of synchronous machines," in *Proc. IEEE Power & Energy Soc. Gen. Meeting (PESGM)*, 2020, pp. 1–5.
[21] "IEEE guide for test procedures for synchronous machines including acceptance and performance testing and parameter determination for dynamic analysis," *IEEE Std 115-2019 (Revision of IEEE Std 115-2009)*, pp. 1–246, 2020.
[22] B. Alves, "Average retail electricity prices in the United States from 1990 to 2021. Statista," https://www.statista.com/statistics/183700/us-average-retail-electricity-price-since-1990/, 2022.
[23] J. Arrillaga and C. P. A. , *Computer Analysis of Power Systems*, 1st ed. Wiley, 1990, iSBN: 0471927600.
[24] "Rotating electrical machines - Part 1: Rating and performance," *IEC 60034-1:2022*, pp. 1–161, 2022.
[25] "Rotating electrical machines - Part 2-3: Specific test methods for determining losses and efficiency of converter-fed ac motors," *IEC 60034-2-3:2020*, pp. 1–54, 2020.
[26] P. Kundur, "Power system stability and control," Toronto, 1993.
[27] J. R. B. Jan Machowski; Zbigniew Lubosny, Janusz W. Bialek, *Power System Dynamics: Stability and Control*, 3rd ed. Chichester: Wiley, 2020, iSBN:1119526345.
[28] J. K. Nøland, E. F. Alves, A. Pardini, and U. Lundin, "Unified reduced model for a dual-control scheme of the high-speed response brushless excitation system of synchronous generators," *IEEE Trans. Ind. Electron.*, vol. 67, no. 6, pp. 4474–4484, 2020.

Yannick Cyiza Karekezi (S'21) was born in Kigali, Rwanda, in 1996. He received the M.Sc. degree in electric power engineering from the Norwegian University of Science and Technology (NTNU), Trondheim, Norway, in 2021. Since then, he has been pursuing a Ph.D. degree at the Department of Electric Power Engineering (IEL) at NTNU. In addition, he is also a part-time scientific assistant with the Department of Electrical engineering, Information Technology and Cybernetics at the University of South-Eastern Norway (USN). Mr. Karekezi regularly serves as a reviewer for the journals IEEE TRANSACTIONS ON ENERGY CONVERSION and the IEEE TRANSACTIONS ON INDUSTRIAL ELECTRONICS. His current research interests include saturation, salient-pole synchronous generators, and power system dynamics. Mr. Karekezi has been a Board Member of the IEEE Power and Energy Society (PES) Norwegian Chapter since 2021.

Emil Ghieh Melfald received the M.Sc. degree in electrical power engineering from the University of South-Eastern Norway (USN), Norway, in 2020. Since 2021, he has been pursuing a Ph.D. degree at the Department of Electrical engineering, Information Technology and Cybernetics (EIK) at USN. His current research interest include machine learning approaches to hydropower applications.

Thomas Øyvang (S'17–M'19) received the Ph.D. degree in Process, Energy and Automation from the University of South–Eastern Norway (USN) in 2018. Since January 2019 he has been an Associate Professor, and the R&D manager for the research group Electrical Power Systems (EPS) with the USN, Porsgrunn. Dr. Øyvang is currently the project manager of the project "System Optimization between power producer and grid owners for more efficient system services (SysOpt)" supported by The Research council of Norway. His research interests include control systems, salient-pole synchronous generators, and power system dynamics. Dr. Øyvang is a Board Member of the Norwegian Academic Committee of Publication in Technology.

Jonas Kristiansen Nøland (S'14-M'17-SM'22) was born in Drammen, Norway, in 1988. He received the M.Sc. degree in electric power engineering from the Chalmers University of Technology, Gothenburg, Sweden, in 2013, and the Ph.D. degree in engineering physics from Uppsala University, Uppsala, Sweden, in 2017. Since 2018, he has been an Associate Professor with the Department of Electric Power Engineering, Norwegian University of Science and Technology. He is also currently an Associate Professor II with the Department of Electrical engineering, Information Technology, and Cybernetics at the University of South-Eastern Norway (USN) and the communication manager of the hydropower systems project SysOpt supported by The Research Council of Norway (RCN). His current research interests include excitation systems, hydrogenerators, large AC machines, and enhancing their utilization. Dr. Nøland serves as an Associate Editor for the IEEE TRANSACTIONS ON ENERGY CONVERSION and the IEEE TRANSACTIONS ON INDUSTRIAL ELECTRONICS, and as the Chair of the IEEE Power and Energy Society (PES) Norwegian Chapter since 2022.